THE JOURNAL OF PHYSICAL CHEMISTRY B

ARTICLE

pubs.acs.org/JPCB

Fast Field-Cycling NMR Relaxometry Study of Chiral and Nonchiral Nematic Liquid Crystals

P.J. Sebastião,[*,†] A. Gradišek,[‡] L. F. V. Pinto,[§] T. Apih,[*,‡,∥] M. H. Godinho,[*,§] and M. Vilfan[‡]

[†]Centro de Física da Matéria Condensada, Av. Prof. Gama Pinto 2, 1649-003 Lisbon, Portugal and Department of Physics, Instituto Superior Técnico, Technical University of Lisbon, Av. Rovisco Pais, 1049-001 Lisbon, Portugal

[‡]Jožef Stefan Institute, Jamova 39, SI-1000 Ljubljana, Slovenia

[§]CENIMAT/I3N, Departamento de Ciência dos Materiais, Faculdade de Ciências e Tecnologia, UNL, 2829-516 Caparica, Portugal

[∥]EN-FIST Centre of Excellence, Dunajska 156, SI-1000 Ljubljana, Slovenia

Supporting Information

ABSTRACT: We present a proton NMR relaxometry study of the molecular dynamics in three liquid crystalline systems: 4′-*n*-pentyl-4-cyanobiphenyl (5CB), (*S*)-4′-(3-methylpentyl)-4-cyanobiphenyl (5CB*), and a 12% weight mixture of 5CB* in 5CB. The proton spin−lattice relaxation time (T_1) was measured as a function of temperature and Larmor frequency in the isotropic, nematic, chiral nematic (N*), and smectic A phases of these liquid crystalline systems. A unified relaxation model was used to analyze the molecular dynamics, considering local molecular rotations/reorientations, translational self-diffusion, and collective motions as the relaxation mechanisms that contribute most effectively to the T_1^{-1} relaxation. Additionally, in the chiral nematic phase a fourth relaxation mechanism associated with the rotations induced by the translational diffusion along the helical axis (RMTD) was included in the model. All experimental results were consistently analyzed taking into account the physical parameters known for 5CB. The global analysis of the experimental results shows that the RMTDs are associated with the pitch value measured for the N* phases and that its contribution to the T_1^{-1} dispersion is observed at low frequencies. The T_1^{-1} dispersion in the smectic A phase of 5CB* is strongly dominated by the layer undulations relaxation mechanism over a broad frequency range from the low kilohertz regime to tens of megahertz. It was the first time such behavior was observed in a low molecular weight liquid crystalline system.

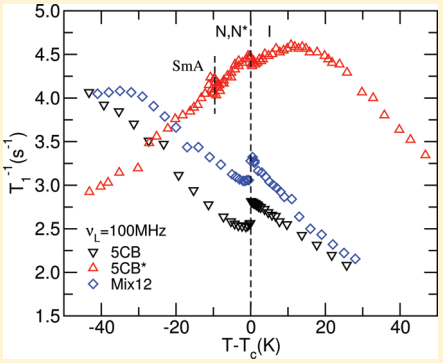

INTRODUCTION

In the last years, the molecular dynamics in nematic (N), smectic A (SmA), C, and C*, reentrant nematic and smectic A phases, twist grain boundary phases A and C—to mention just a few liquid crystalline systems—were studied in detail by proton NMR relaxation.[1−3] In contrast, very few NMR relaxometry studies have been performed in chiral nematic phases (N*) with enough detail to reveal the effects of specific N* phase structure on molecular motions. The initial molecular dynamics studies in chiral nematic phases[4−6] have shown that the general spin−lattice relaxation processes are similar to those observed in the pure nematic compounds and that the helical twist of the nematic director characteristic of these mesophases might affect the relaxation at low frequencies in view of the correlation time associated with the rotations induced by the translational diffusion along the helical axis (RMTD).[6]

This specific relaxation mechanism was considered for the analysis of the longitudinal proton relaxation time dispersion results of a cholesteric liquid crystalline estradiol (named BET).[7] A surprising feature of that analysis was that to explain the results authors[7] had to assume that in the T_1^{-1} model the relaxation mechanism corresponding to the collective motions (CM) in the N* phase had a $(T_1^{-1})_{CM} \sim \nu^{-1}$ law and not the expected square-root frequency dependence law found in nematic phases in the absence of local smectic order.[1,2,6] More recently, the molecular dynamics in the chiral nematic phase of a chiral compound (named HZL 7/*) that presents TGB phases was studied by proton NMR relaxometry.[3] The results for the N* phase of that compound were analyzed taking into account both the $(T_1^{-1})_{CM} \sim \nu^{-1/2}$ and RMTD contributions.[3] In neither BET nor HZL 7/* proton NMR relaxation studies was the helical pitch reported, and the correlation time of the RMTD contribution could not be correlated with the helical pitch of the chiral phase as required by the RMTD model.[6]

Additional motivation to gain a more detailed knowledge of the molecular dynamics in the cholesteric phases is the potential contribution to the optimization of chiral liquid crystalline systems suitable for new electro-optical applications, such as self-assembled microlasers in photonics.[8] Some of these applications

Received: July 7, 2011
Revised: September 24, 2011
Published: October 17, 2011

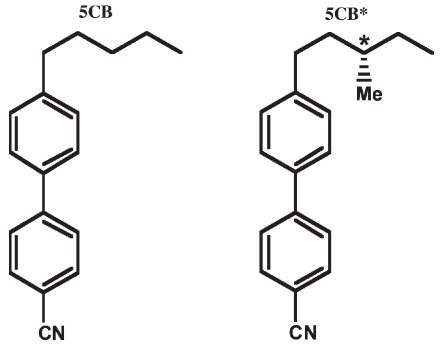

Figure 1. 5CB and 5CB* chemical structures.

require a fine-tuning of the helical pitch accomplished with the appropriate mixing nematic and cholesteric liquid crystals (LCs).

In this work, we report a detailed study of the molecular dynamics in three liquid crystalline systems: the pure nematic liquid crystal 4′-*n*-pentyl-4-cyanobiphenyl (5CB), the pure chiral nematic compound (*S*)-4′-(3-methylpentyl)-4-cyanobiphenyl (5CB*),[9] and a mixture of 5CB* in 5CB. The two systems 5CB and 5CB* have similar molecular structures, the only difference being the chiral center in the 5CB* aliphatic chain, as can be seen in Figure 1.

Due to the resemblance between the two LCs, the possibility to obtain a N* phase in a temperature range around room temperature and to tune the helical pitch in the N* to measurable values by an appropriate choice of the LC mixtures, we were able to perform a detailed study of the molecular dynamics in the N* phase and to test the existing relaxation models, taking the comprehensive knowledge about the 5CB LC physical properties into account.

The ^{1}H spin−lattice relaxation time was measured as a function of temperature for a selected Larmor frequency $\nu_L = \omega/2\pi$ of 100 MHz and as a function of the ν_L for a few selected temperatures in all phases of the three liquid crystalline systems.

EXPERIMENTAL SECTION

Systems Description. The LC systems studied were: the nematic liquid crystal 4′-*n*-pentyl-4-cyanobiphenyl (5CB), the chiral nematic compound (*S*)-4′-(3-methylpentyl)-4-cyanobiphenyl (5CB*), which presents a chemical structure very similar with 5CB, and a 12% w/w mixture of 5CB* in 5CB, hereafter referred to as Mix12. The 12% (w/w) concentration was chosen to produce a helical pitch detectable by polarizing optical microscopy (POM). The small concentration of 5CB* lowered the clearing point temperature (T_c) just a few degrees below the isotropic−nematic transition temperature (T_{IN}) of pure 5CB.

5CB* presents a N* phase between 259 and 251 K,[9] and a smectic A phase is reported for temperatures below 251 K. The crystallization temperature is not reported in ref 9. The LC mixture Mix12 presents a I−N* phase transition at 302 K (obviously lower than the T_{IN} = 307 K measured for 5CB).

5CB* was first reported by Gray et al.[9] It presents a chiral nematic phase below room temperature over a broad temperature range and a helical pitch of about 0.3 μm. As can be observed in Figure 1, the difference between the two compounds is a methyl group that replaces one hydrogen at the C3 position of the pentyl carbon chain.

The 5CB* compound was synthesized using the following seven-step procedure:

1. Synthesis of (*S*)-2-methylbutyl 4-methylbenzenesulfonate;[10]
2. Synthesis of (*S*)-3-methylpentanenitrile;[10]
3. Synthesis of (*S*)-3-methylpentanoic acid;[10]
4. Synthesis of (*S*)-3-methylpentanoyl chloride;
5. Synthesis of (*S*)-1-(4′-bromobiphenyl-4-yl)-3-methylpentan-1-one;
6. Synthesis of (*S*)-4-bromo-4′-(3-methylpentyl)biphenyl;
7. Synthesis of (*S*)-4′-(3-methylpentyl)biphenyl-4-carbonitrile.

The synthesis is detailed in the Supporting Information. Due to the enhanced yield of the new synthesis procedure, it was possible to obtain a sufficient amount of 5CB* to prepare all necessary NMR samples.

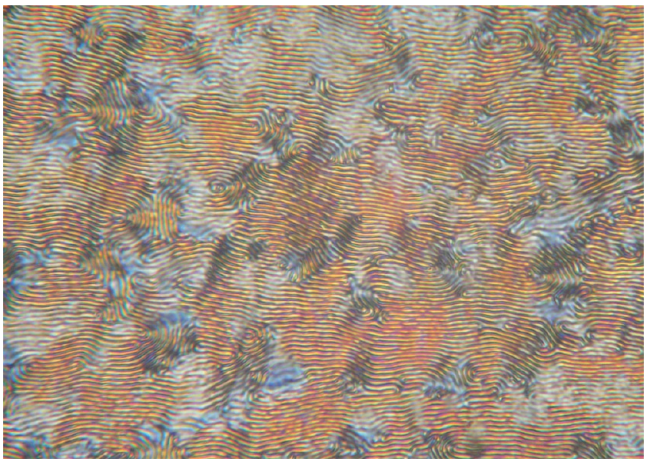

Figure 2. POM, between cross-polarizers, texture of the chiral nematic phase at T = 301 K of the 12% (w/w) mixture of 5CB* in 5CB. The pitch value is 3.3 μm.

The chiral nematic texture observed by polarizing optical microscopy, between cross-polarizers, at 301 K is shown in Figure 2. The pitch value is 3.3 μm. The POM studies were conducted on a polarizing optical microscope Olympus BH2 coupled to a Casio EX-F1 Exilim Pro photocamera.

Experimental Details. The measure of the spin−lattice relaxation time over a broad frequency range (5 kHz−100 MHz) requires the use of both fast field-cycling and classical inversion−recovery experimental NMR techniques. Due to signal-to-noise limitations, the standard inversion−recovery techniques can in practice be used only for Larmor frequencies above 4 MHz. Below this frequency, fast field-cycling relaxometry techniques are used to measure T_1. The proton's spin system is subjected to fast changes of the external magnetic field that produce an evolution of the magnetization at the desired magnetic field (B_E), characterized by T_1 (B_E), and the detection of the resonance radio frequency signal is always made at a fixed magnetic field ($B_D > B_E$). The signal-to-noise limitations associated with the NMR signal detection are overcome with this technique because the free-induction decay signal is always aquired at a reasonably high resonance frequency $\nu_L = \gamma B/2\pi$, in the present study 9.25 MHz.[11,12]

The relaxation dispersion data were acquired using the Fast Field Cycling NMR relaxometer SPINMASTER FFC-2000 (Stelar s.l.r.). About 500 of each sample was used for the measurements. The longitudinal spin−lattice relaxation time T_1 of protons was measured in the the frequency range from 18 MHz to 5 kHz. In addition, T_1 was measured at 100 MHz using a standard NMR spectrometer. For each of the samples, the dispersion was measured at temperatures 5 K above and below

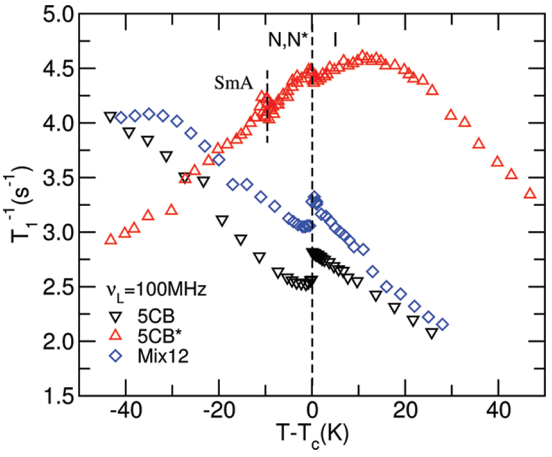

Figure 3. Spin−lattice relaxation time as a function of temperature for 5CB, 5CB*, and Mix12 (mixture of 12% (w/w) of 5CB* in 5CB) for ν_L = 100. $T_c^{5CB} = T_{IN} = 307$, $T_c^{5CB*} = T_{IN^*} = 259$, and $T_c^{Mix12} = T_{IN^*} = 302$.

the isotropic−nematic or isotropic−chiral nematic phase transitions. Temperature was controlled with a standard gas flow system with a precision of ±0.1°. To achieve temperatures below room temperature, the air was first led through a liquid nitrogen container to cool. For frequencies higher than 8 MHz, a non-prepolarized pulse sequence (NPS) was used, while below that frequency relaxation times were obtained using a prepolarized pulse sequence (PPS). The prepolarization and acquisition frequencies were 18.00 and 9.25 MHz, respectively. A 6.5 μs proton 90° pulse was used. All other parameters were optimized according to each experiment. Additionally, the temperature dependencies of proton T_1 were measured at the Larmor frequency of 100 MHz over a wide temperature range with a home-built NMR spectrometer and an Oxford magnet. The inversion recovery pulse sequence with a 4.5 μs 90° pulse was used.

Experimental Results. The experimental results for the spin−lattice relaxation rate as a function of temperature and as a function of the Larmor frequency are presented in Figure 3 and Figure 4.

In the case of the pure 5CB*, additional T_1^{-1} dispersion data were obtained in the isotropic phase at 307 K and in the SmA phase at 245 K. These results are shown in Figure 5.

As it can be observed in Figure 3, the phase transitions are detected as discontinuities in $T_1^{-1}(T)$.

The T_1^{-1} dispersions at 5 K below T_c are different for all systems, as can be observed in Figure 4b. In the case of Mix12, the T_1^{-1} values are larger than the ones measured for the pure 5CB at all frequencies although both systems present similar T_1^{-1} frequency dependencies.

The experimental T_1^{-1} dispersions of 5CB* shown in Figure 5 corresponding to $T_{I-N^*} \pm 5$ K are very similar. The T_1^{-1} dispersion of 5CB* in the SmA is slightly different from the one observed in the N* phase in the low frequency region. The observed monotonous decrease of T_1^{-1} with increasing frequency in the broad frequency range from a few kilohertz up to 100 MHz is quite interesting. In fact, in low molecular weight liquid crystals the T_1^{-1} dispersion in the SmA phase most often presents a plateau in the intermediate frequency range, between the tens of kilohertz and the megahertz range.[13−15] However, we note that a similar continuous decrease of T_1^{-1} with increasing frequency in this frequency range has been observed in the smectic A phase of tetrapode molecules.[2,16]

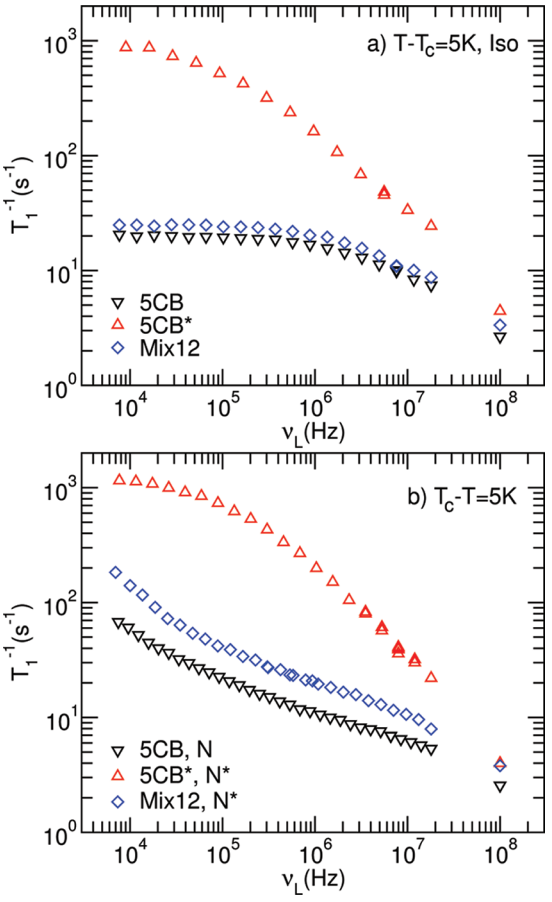

Figure 4. Spin−lattice relaxation time as a function of Larmor frequency, for 5CB, 5CB*, and Mix12: *(a) 5 K above the clearing point temperature and (b) 5 K below the clearing point temperature.

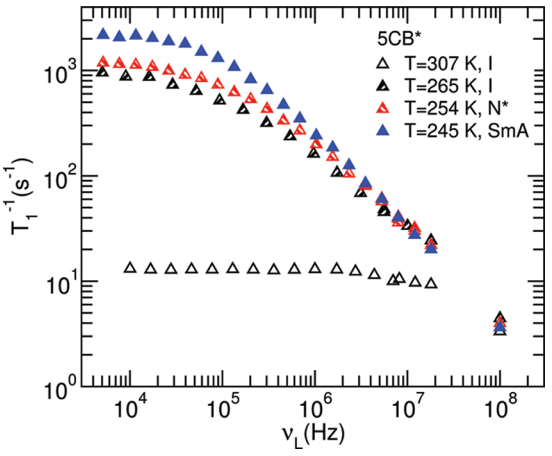

Figure 5. Spin−lattice relaxation time as a function of Larmor frequency for 5CB* in the isotropic phase (307 and 265 K), chiral nematic phase (254 K), and smectic A phase (245 K).

The self-diffusion coefficients in the isotropic phase, D_{iso}, of 5CB* and 5CB/5CB* samples have been determined from the diffusion-induced attenuation of the ^{1}H NMR spin−echo in a static fringe field (SFF) of a superconducting magnet.[17] The samples were fine-positioned at one edge of a superconducting coil with a center field of 400 MHz (9.4 T). The proton

dx.doi.org/10.1021/jp206429j |J. Phys. Chem. B 2011, 115, 14348–14358

resonance frequency at the sample was 200 MHz, and the magnetic field gradient was 68 T/m. The stimulated spin−echo pulse sequence was used. The diffusion coefficient was determined as described in ref 18. This experimental setup did not allow for the measurement of $D_\perp$ and $D_\parallel$ in the chiral nematic phases of both 5CB* and Mix12 systems.

RELAXATION MECHANISMS

The proton spin−lattice relaxation rate reflects the modulation of the interproton dipolar interaction by the molecular motions. The interproton spin distance and/or the angle between the interproton vector and the magnetic field vary when molecules move. Proton spin−lattice relaxation is affected by the fluctuations of *intramolecular* as well as *intermolecular* interactions and is therefore sensitive to both local rotations/reorientations and translational self-diffusion motions. These motions are usually characterized by short correlation times of the order of $10^{-11} - 10^{-9}$s. In the case of liquid crystalline phases, relaxation processes with long correlation times, associated with order director fluctuations, can also be present.[1,2]

The effects of these relaxation mechanisms depend both on temperature and Larmor frequency. In the analysis of T_1^{-1}, we will consider the following relaxation mechanisms:

(i) Translational self-diffusion (SD) is a molecular motion affected by the local phase structure. In the isotropic phase of bulk liquid crystals $(T_1^{-1})_{SD}$ can be calculated analytically using the model of Torrey[19] that depends on the spin density n, the self-diffusion constant D_{iso}, the mean square jump distance $\langle r^2 \rangle$, and the width of the molecules d. This model was extended numerically for the nematic and smectic A phases by Žumer and Vilfan[20,21] to consider the anisotropy of the self-diffusion through the two diffusion constants $D_\perp$ and $D_\parallel$.

(ii) Local molecular rotations/reorientations (R) of liquid crystal molecules usually consider the rotations along the long molecular axis and reorientations around the short molecular axis, with correlation times τ_L and τ_S, respectively. The model of Woessner[22] is often used to calculate the contribution of rotations to the relaxation rate in the isotropic phase. For nematic and smectic A phases, the Woessner model can be extended taking into consideration the rotational motions' restrictions that result from the increased orientational order in these mesophases. $(T_1^{-1})_R$ is also expressed as a function of the nematic order parameters S and $\langle P_4 \rangle$.[23,24] The intramolecular interproton distances and interproton vector angles with respect to the long molecular axis are also included in the form of an averaged weight factor.[2]

(iii) Order director fluctuations (ODF) correspond to orientational fluctuations of the nematic director with respect to its time-average orientation. They reflect the collective reorientational motion of molecules that can be expressed in terms of a distribution of the fluctuation modes with mean square amplitudes $\langle |n(\mathbf{q})|^2 \rangle$ and relaxation times $\tau(\mathbf{q})$ that depend on the viscoelastic parameters of the system. These collective motions can be observed in N, N*, SmA, and SmC phases.[2,15,25]

In addition to the distribution of the fluctuation modes, the $(T_1^{-1})_{ODF}$ model takes into account the maximum and minimum wave vectors limits, $\mathbf{q}_{max}$ and $\mathbf{q}_{min}$, associated with the molecular width d and the coherence length ξ, respectively. Assuming the one-constant approximation for the elastic constants and viscosities,[26] the limits of the modes' relaxation times can be expressed as $\tau_{max}(q_{min}) \sim \eta\xi^2/(4\pi^2 K)$ and $\tau_{min}(q_{max}) \sim \eta d^2/(4\pi^2 K)$, where η is an effective viscosity and K the elastic constant. These limits are usually presented as the cutoff frequencies $\omega_{ODFmax} = 1/\tau_{min}$ and $\omega_{ODFmin} = 1/\tau_{max}$ of the well-known $(T_1^{-1})_{ODF} \sim \omega^{-1/2}$ frequency dependence. This contribution was initially proposed for the nematic phase by Pincus and first confirmed experimentally by Noack et al.[27,28]

$(T_1^{-1})_{ODF}$ can be written as

$$\left(\frac{1}{T_1}\right)_{ODF} = \frac{A_{ODF}}{\omega^{1/2}}\left[f\left(\frac{\omega_{ODFmax}}{\omega}\right) - f\left(\frac{\omega_{ODFmin}}{\omega}\right)\right] \quad (1)$$

where $f(x)$ is the cutoff function,[1] and the prefactor

$$A_{ODF} = (9/8)(\mu_0/4\pi)^2\gamma^4\hbar^2 k_B T S^2 \eta^{1/2}/(\sqrt{2}\pi K^{3/2} a_{eff}^6)$$

a_{eff}^{-6} depends on the interproton distances and interproton vector angles with respect to the long molecular axis.[24] η and K are the viscosity and elastic constant in the one-constant approximation of the viscoelastic properties of the nematic liquid crystal.

In the isotropic phase just above T_{IN} a contribution to the relaxation rate with a square-root power law can appear as well. This contribution is associated with *local order fluctuations* (OF)

$$\left(\frac{1}{T_1}\right)_{OF} = \frac{A_{OF}}{\omega^{1/2}}\int_{\omega_{OFmin}/\omega}^{\omega_{OFmax}/\omega} \frac{\sqrt{x}}{1 + (x + \omega_0/\omega)^2}\,dx \quad (2)$$

with $A_{OF} = (9/8)(\mu_0/4\pi)^2\gamma^4\hbar^2 k_B T \eta_{iso}^{1/2}/(4\pi^2 K_{iso}^{3/2} a_{eff}^6)$. ω_{OFmin} and ω_{OFmax} are the low and high cutoff frequencies that correspond to the largest and smallest wavelength modes, respectively. $\omega_0 \sim K_{iso}/\eta\xi^2$ depends on the coherence length, ξ, associated with the size of nematic cybothatic domains in the isotropic phase and acts also as a cutoff frequency in eq 2.[1] It is worth to mention that numerically $(T_1^{-1})_{OF}$ and $(T_1^{-1})_{ODF}$ can produce similar fitting curves although with different model parameter values.

In the SmA phase, *order director fluctuations* are restricted by the layered structure of the phase. The fluctuation modes are associated with pure splay deformations in the layer planes. These fluctuations are known as *layer undulations* (LU)[1,26]

$$\left(\frac{1}{T_1}\right)_{LU} = \frac{A_{LU}}{\omega\pi}\left[\arctan\left(\frac{\omega_{ODFmax}}{\omega}\right) - \arctan\left(\frac{\omega_{ODFmin}}{\omega}\right)\right] \quad (3)$$

with $A_{LU} = 9\,\mu_0^2\gamma^4\hbar^2 k_B T S^2/(16\pi a_{eff}^6 \xi_z K_1)$, where ξ_z is the correlation length of undulations and K_1 is Frank's splay elastic constant.[13] $(T_1^{-1})_{LU}$ has a distinct frequency dependence with a power law $(T_1^{-1})_{LU} \sim \omega^{-1}$ for frequencies $\omega_{ODFmin} < \omega < \omega_{ODFmax}$.

(iv) Rotations mediated by translational displacements (RMTD) are a particular type of motions that, in the case

dx.doi.org/10.1021/jp206429j |J. Phys. Chem. B 2011, 115, 14348–14358

of chiral nematic phases, are associated with the molecular diffusion along the chiral nematic helical axis. RMTD in chiral nematic phases can be an effective relaxation mechanism with a model proposed by Vilfan et al.[6] The correlation time for this motion is $\tau_{RMTD} = p^2/(16\pi^2 D_\perp)$ and depends on the diffusion constant $D_\perp$ and on the helical pitch p. This mode depends also on an effective interproton distance r_{eff}.

The details of the model can be found in the Supporting Information.

ANALYSIS OF T_1^{-1} EXPERIMENTAL RESULTS AND DISCUSSION

The model used to analyze the experimental spin−lattice relaxation results considers the sum of contributions to T_1^{-1} taking into account the particular structure of each liquid crystalline phase. Usually, it is assumed that these contributions are statistically independent and/or have distinct characteristic time scales. Therefore, any cross-term contribution to the total relaxation rate is assumed to be negligible.[1,2,28] The general expression for the total relaxation rate considered in this work has the form

$$\left(\frac{1}{T_1}\right) = \left(\frac{1}{T_1}\right)_R + \left(\frac{1}{T_1}\right)_{SD} + \left(\frac{1}{T_1}\right)_c + \left[\left(\frac{1}{T_1}\right)_{RMTD}\right]_{N^*} \quad (4)$$

where index c refers to the type of collective motions: OF, ODF, or LU. In the case of the nematic and smectic A phases, the RMTD contribution is not present, and the contribution of the slow collective motions is given by the $(T_1^{-1})_{ODF}$ and $(T_1^{-1})_{LU}$ models: eq 1 and eq 3, respectively. In the isotropic phase, the order fluctuations observed for temperatures above the T_{IN} (or T_{IN^*}) transition are expressed by eq 2.

The $(T_1^{-1})_R$ depends on S, τ_S, and τ_L, which are temperature dependent. The rotation/reorientation mechanism is thermally activated, and therefore both τ_S and τ_L have temperature dependencies described by Arrhenius-type laws

$$\tau_S = \tau_{S,T_{ref}} \exp(E_S R^{-1}(T^{-1} - T_{ref}^{-1})) \text{ and}$$

$$\tau_L = \tau_{L,T_{ref}} \exp(E_L R^{-1}(T^{-1} - T_{ref}^{-1}))$$

with E_S and E_L being the activation energies of τ_S and τ_L, respectively. T_{ref} is the temperature used as a reference, that is, the temperature at which the T_1^{-1} dispersion was obtained in each phase. In addition, it is necessary to consider the prefactor $A_R = 9\,\mu_0^2\gamma^4\hbar^2 a_R/(128\pi^2)$ where the corrective factor a_R is included to take into account the contribution of dipolar interactions between intermolecular proton spins and the contributions of next-to-the-nearest neighbors spin pairs. The nematic order parameter is also temperature dependent, and in the case of 5CB it was obtained from the literature[29] as previously referred. In the case of 5CB* and Mix12, it was assumed that the order parameter has a temperature dependence identical to that of 5CB in view of the similarity between the 5CB and 5CB* molecules.

The $(T_1^{-1})_{SD}$ depends on the spin density n that was assumed to be temperature independent and estimated for the three systems on the basis of a density of 1 kg/m^3. $n = 4.59 \times 10^{28}$ m^{-3}, $n = 4.8 \times 10^{28}$ m^{-3}, and $n = 4.64 \times 10^{28}$ m^{-3} were estimated for 5CB, 5CB*, and Mix12 liquid crystalline systems, respectively. $d = 5$ was assumed for all molecules.

The translational self-diffusion coefficients D_{iso} measured for different temperatures in the isotropic phase of 5CB* and Mix12 LC systems are presented in Figure 6. These results were analyzed using Arrhenius expressions of the type $D_{iso} = D_{T_{ref}} \exp(-E_D R^{-1}(T^{-1} - T_{ref}^{-1}))$ making it possible to use the interpolated values for the analysis of the $(T_1^{-1})_{SD}$ temperature dependence. The results were also used to extrapolate the values of self-diffusion constant in the N* and SmA phases of 5CB* and in the N* of the Mix12 considering that

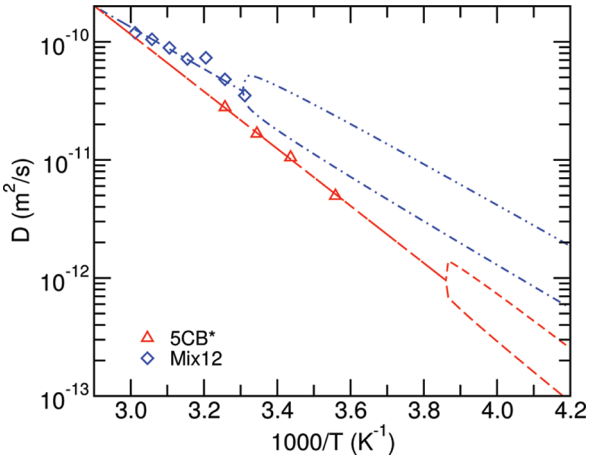

Figure 6. Translational self-diffusion constant obtained as a function of temperature in the isotropic phases of 5CB* and of the Mix12 mixture. *The dashed (red)* and *dot-dashed (blue)* curves represent a model fit to the experimental data of 5CB* and Mix12 LC systems. The curves are extrapolated into the mesophases of both systems at lower temperatures. In the N and N* phases, the diffusion constant splits in $D_\parallel$ e $D_\perp$.

$$\begin{aligned} D_\parallel &= \langle D \rangle [1 + 2S(1-\rho)/(2\rho + 1)] \\ D_\perp &= \langle D \rangle [1 - S(1-\rho)/(2\rho + 1)] \end{aligned} \quad (5)$$

with $\langle D \rangle = (2D_\perp + D_\parallel)/3 \sim D_{iso}$. $\rho = \pi d/(4\ell)$, where d and ℓ are the molecular width and the molecular length, respectively.[29] Since both 5CB and 5CB* have similar values of ℓ and d, $\rho \simeq 0.2$. Assuming further that $S = (1 - T/T^*)^\gamma$ with $T^* \sim T_{IN,IN^*}$[30] and with $\gamma = 0.162$ identical for the studied LC systems, the fit curves to the experimental self-diffusion data were calculated also for temperatures below T_{IN^*} as shown in Figure 6.

The self-diffusion coefficients of 5CB for different temperatures were estimated considering the values obtained by Dvinskikh et al. with activation energies $E_D^{\langle D \rangle} \simeq E_D^{iso} \simeq 32.8$ kJ mol^{-1}.[29] $D_{307K}^{5CB*} \simeq 2.8 \times 10^{-11}$ m^2 s^{-1} and the activation energy $E_D^{5CB*} = 46 \pm 2$ kJ mol^{-1} K^{-1} were obtained for the 5CB* compound in the isotropic phase. $D_{307K}^{mix} \simeq 4.7 \times 10^{-11}$ m^2 s^{-1} and the activation energy $E_D^{mix} = 33.9 \pm 0.9$ kJ mol^{-1} K^{-1} were obtained for the Mix12 mixture. In both 5CB* and Mix12 liquid crystals, it was assumed that the activation energies of the self-diffusion coefficients in the mesophases of both systems were similar to the ones obtained in the isotropic phase.

For 5CB, the values obtained from the literature are $D_{313K}^{5CB} \simeq 5.4 \times 10^{-11}$ m^2 s^{-1}, $E_a^{5CB} = 32.8 \pm 0.5$ kJ mol^{-1} K^{-1} in the isotropic phase, and $D_{303K}^{5CB} \simeq 4.1 \times 10^{-11}$ m^2 s^{-1} and $E_a^{5CB} = 29 \pm 2$ kJ mol^{-1} K^{-1} in the nematic phase.[29]

The relaxation rate model for the collective motions $(T_1^{-1})_{OF|ODF|LU}$ depends on the prefactor $A_{OF|ODF|LU}$ and on the high and low cutoff frequencies, $\omega_{OF|ODF|LUmax}$ and $\omega_{OF|ODF|LUmin}$, respectively. In addition, the $(T_1^{-1})_{OF}$ model

dx.doi.org/10.1021/jp206429j | J. Phys. Chem. B 2011, 115, 14348–14358

Table 1. Model Parameters Obtained from the Best Fits of Equation 6 to the Experimental T_1^{-1} Results in the Isotropic and Nematic Phases of 5CB[a]

phase	I	N
T (K)	313	303
τ_S (10^{-9} s)	1.6 ± 0.2	1.34 ± 0.07
τ_L (10^{-10} s)	4.5 ± 0.4	6.8 ± 0.3
A_R (10^{-49} m^6 s^{-2})	3.6	3.6
$\langle r^2 \rangle$ (10^{-20} m^2)	16 ± 4	-
A_c (10^3 s$^{-3/2}$)	15.6 ± 0.4	12.9 ± 0.3
$\omega_0/2\pi$ (10^3 Hz)	459 ± 20	-
$\omega_{cmin}/2\pi$ (10^3 Hz)	0	<1
$\omega_{cmax}/2\pi$ (10^8 Hz)	~0.4	~1

[a] Index c refers to the type of collective motions observed in each phase: local order fluctuations, OF, in the isotropic phase and order director fluctuations, ODF, in the nematic phase.

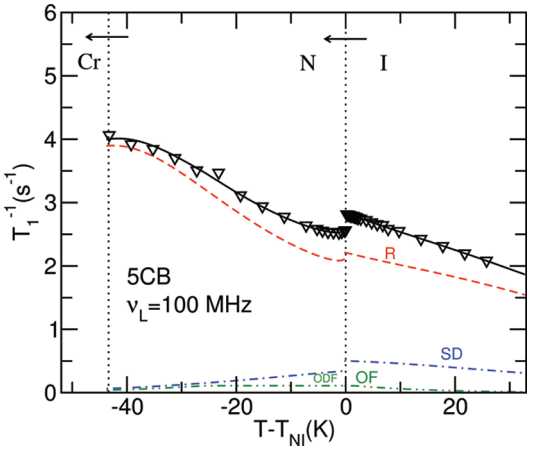

Figure 7. Experimental results of T_1^{-1} as a function of temperature and the best model fit curves obtained with the relaxation model given by eq 6 as explained in the text.

also depends on the coherence-dependent cutoff frequency ω_0 associated with the cybothatic clusters.

The T_1^{-1} model given by eq 4 was fitted to the experimental results using a home-written nonlinear fitting software package,[31] considering a global minimum least-squares target for each LC system. In all phases, the model fitting was performed considering simultaneously the temperature- and frequency-dependent T_1^{-1} experimental results.

5CB Data Analysis. The 5CB T_1^{-1} dispersion and temperature dependence in all phases were analyzed taking into account the model

$$\left(\frac{1}{T_1}\right) = \left(\frac{1}{T_1}\right)_R + \left(\frac{1}{T_1}\right)_{SD} + \left(\frac{1}{T_1}\right)_{OF|ODF} \quad (6)$$

and the model free parameters: A_R, τ_S, E_S, τ_L, E_L, $\langle r^2 \rangle_{iso}$, A_c, ω_{cmax}, and ω_{cmin}. The values of the remaining model parameters were obtained from the literature as explained before. The whole spin−lattice relaxation analysis of the 5CB liquid crystal is necessary to test the relaxation model considered here before analyzing the experimental results for the 5CB* and Mix12 LC systems.

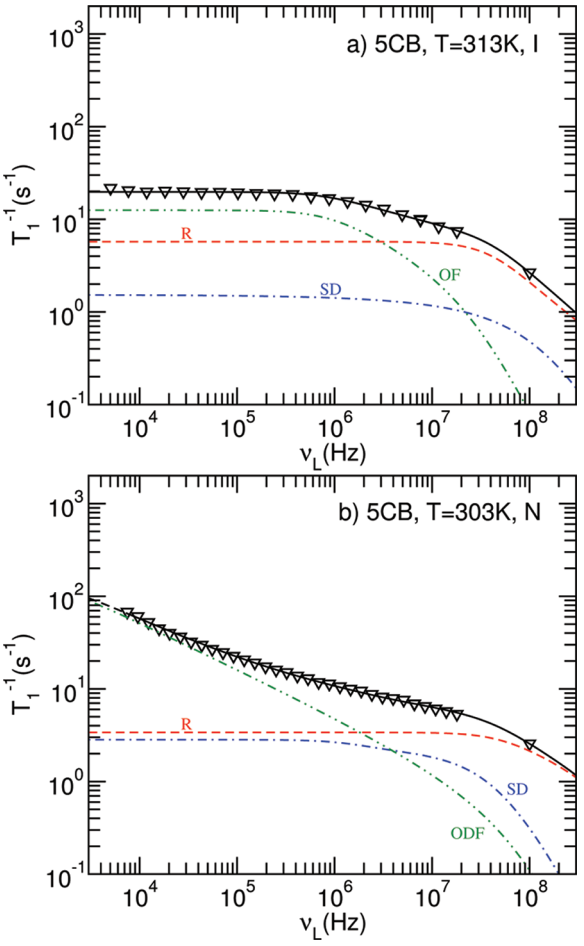

Figure 8. Experimental T_1^{-1} dispersion results for 5CB and the best model fit curves obtained with the relaxation model given by eq 6 as explained in the text: (a) isotropic phase and (b) nematic phase.

The best fits obtained with the model parameters presented in Table 1 are shown in Figure 7 and Figure 8, for one temperature in each 5CB phase. The activation energies obtained are E_S = (29 ± 14) kJ mol^{-1} K^{-1}, E_L = (40 ± 7) kJ mol^{-1} K^{-1} in the isotropic phase and E_S < 20 kJ mol^{-1} K^{-1}, E_L = (33 ± 3) kJ mol^{-1} K^{-1} in the nematic phase.

As can be observed, the T_1^{-1} model interprets all experimental results very well. The analysis of Figure 7 shows that the T_1^{-1} behavior at the isotropic−nematic transition is well explained by the onset of the nematic order and the temperature dependence of the nematic order parameter. In the isotropic phase order, fluctuations start to have some importance close to the transition even at 100 MHz, although they contribute more to relaxation at much lower frequencies as can be observed in Figure 8a. In view of the small importance of OF at high frequencies, it is difficult to estimate the value of the high cutoff frequency. The value $\omega_{ODFmax}/2\pi$ presented in Table 1 presents a reasonable value in the 40−100 MHz range that could be estimated from the global fitting procedure. It should be noted that this value can not correspond to a correlation time $\tau_{min} = 1/\omega_{ODFmax}$ smaller than the minimum of τ_S and τ_L for a given temperature. Therefore, the observed increase of τ_S and τ_L with decreasing temperature must correspond to a decrease of ω_{ODFmax}. In Figure 7, this is seen as a decrease of the contribution of ODF with decreasing temperature.

dx.doi.org/10.1021/jp206429j |J. Phys. Chem. B 2011, 115, 14348–14358

The cutoff frequency ω_0 associated with the coherence length of the cybothatic clusters was estimated with a significant uncertainty since the OF contribution also depends on a low cutoff frequency ω_{OFmin} associated with the largest wavelength fluctuation mode detected. Assuming that the cluster boundaries do not impose limits to the fluctuation modes, it is reasonable to consider $\omega_{OFmin} \sim 0$.

In the nematic phase, the T_1^{-1} temperature dependence at 100 MHz is basically dominated by the rotations/reorientations relaxation mechanism. Both ODF and SD become less important with decreasing temperatures as shown in Figure 7. On the contrary, below 2 MHz ODF is the most important relaxation mechanism as can be seen in Figure 8b. No low cutoff frequency could be estimated for 5CB, as it seems to be smaller than 1 kHz and no reliable T_1^{-1} measurements were made for frequencies below 7 kHz. Therefore, below 7 kHz the fitting curve is represented with a dashed line in Figure 8b. The high cutoff frequency considered in the model fit is ~100 MHz since due to the small contribution of ODF to the T_1 relaxation this value can not be independently estimated from the model fit. Considering the measured values of 5CB viscoelastic parameters $\eta \sim 2.3 \times 10^{-2}$ Pa s,[32] $K \sim 4.5 \times 10^{-12}$ N,[33] considering $S \sim 0.52$,[29] $\ell \sim 17$, and $a_{eff}^{-6} \simeq 6 \times 10^{57}$ m^{-6}, the estimated values of A_{ODF} and $\omega_{ODFmax}/2\pi$ are 15×10^4 s$^{-3/2}$ and 420, respectively, which is clearly compatible with the values obtained from the best model fit presented in Table 1.

The correlation times for the rotational motions are compatible with those obtained from deuteron NMR studies.[34,35] In fact, τ_L for $T = 303$ K is very close to the values estimated from D_z^{-1} and D_R^{-1}, the rotational diffusion constants of the chain and ring deuterons, respectively, along the rings' para axis.[35] The activation energy E_L is smaller than the $E_z^{D_z}$ but larger than $E_R^{D_R}$. Due to spin diffusion the proton spin−lattice relaxation is not site specific; therefore, E_L reflects the motion of the whole molecule, and it is reasonable that its value is in between the values obtained for the chain and rings dynamics.

The τ_S value is slightly lower than the one obtained from the D_x^{-1} results reported by Dong[35] for 5CB-d_{15} NMR chain deuteron studies. An upper limit for the activation energy E_S was estimated here, and its value is smaller than E_L, which is in agreement with the 5CB-d_{15} results.[35] Nevertheless, this value is lower than the value obtained from the deuteron studies, maybe as a consequence of the site-specific nature of the deuteron NMR relaxation versus the global molecular dynamics character associated with the proton interdipolar interaction in proton NMR.

The value of τ_S obtained in the nematic phase for $T = 303$ K is close to the value obtained by Struppe et al.[36] The small difference is related to the use of different relaxation models for the rotations/reorientations mechanism and to fact that in ref 36 the SD mean-square jump time was considered a free fitting parameter and not a parameter estimated from independent measurements of self-diffusion constant.

5CB* Data Analysis. The 5CB* T_1^{-1} dispersions and temperature dependence in all phases were analyzed taking into account the model

$$\left(\frac{1}{T_1}\right) = \left(\frac{1}{T_1}\right)_R + \left(\frac{1}{T_1}\right)_{SD} + \left(\frac{1}{T_1}\right)_{OF|ODF|LU} + \left(\frac{1}{T_1}\right)_{RMTD} \quad (7)$$

and the model free parameters: A_R, τ_S, E_S, τ_L, E_L, $\langle r^2\rangle_{iso}$, A_c, ω_{cmax}, ω_{cmin}, and A_{RMTD}. A fixed value of the pitch $p = 0.3 \times 10^{-6}$ m was considered in the N* phase.[9] In view of the relatively low magnetic field associated with the fast-field cycling measurements ($\leq$0.5 T), it is assumed that the value of the pitch remains constant zfor frequencies below 18 MHz.[26] In view of the large range of temperatures covered in each phase, a linear temperature dependence was considered for the prefactor $A_c(T) \sim A_c^0 + A_c^1(T - T_{IN^*})$ of either local order fluctuations mechanism, order director fluctuations, or layer undulations and for their respective low cutoff frequencies: $\omega_{cmin} \sim \omega_{cmin}^0 + \omega_{cmin}^1(T - T_{IN^*})$. In addition, the order parameter S was calculated assuming the same temperature dependence as for 5CB, and the translational self-diffusion coefficients were extrapolated from the values measured at the isotropic phase. Since the T_1^{-1} temperature dependence measurements were made for a frequency of 100 MHz and it is expected that the RMTD has a negligible contribution at this Larmor frequency, no temperature dependence was considered for the picth.

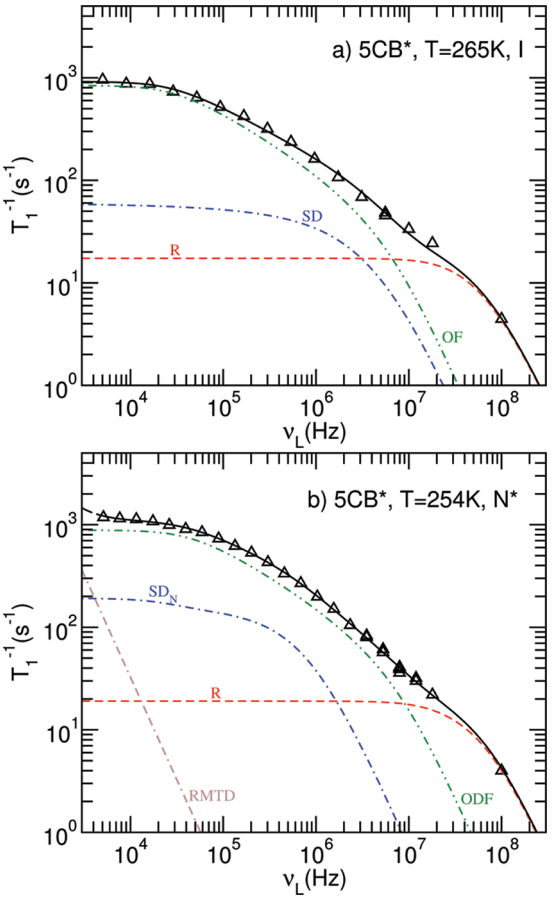

Figure 9. Experimental T_1^{-1} dispersion results and the best model fitting curves obtained with the relaxation model given by eq 7 as explained in the text, for one temperature in isotropic, (a) and nematic (b) phases of 5CB*.

Figure 9−Figure 11 show the model curves obtained from the best fits to the presented experimental results, taking into account both T_1^{-1} frequency and temperature dependencies. The model fit obtained in the isotropic phase of 5CB* at the second temperature 48 K above T_{IN^*} is identical to the one presented in Figure 8a (see the Supporting Information). The fitting parameters of the best fits are presented in Table 2. In addition, the activation energies obtained are $E_S = (2.6 \pm 0.3)$ kJ mol^{-1} K^{-1}, $E_L = (46.8 \pm 0.9)$ kJ mol^{-1} K^{-1} in the isotropic

dx.doi.org/10.1021/jp206429j |J. Phys. Chem. B 2011, 115, 14348–14358

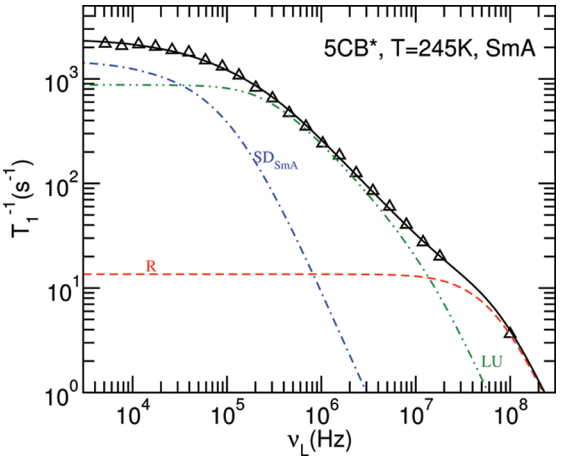

Figure 10. Experimental T_1^{-1} dispersion results and the best model fitting curves obtained with the relaxation model given by eq 7 in the smectic A phase of 5CB*.

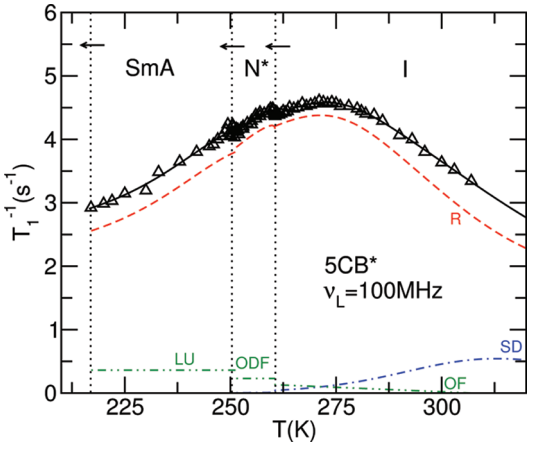

Figure 11. Experimental results of T_1^{-1} as a function of temperature and the best model fit curves obtained with the relaxation model given by eq 7 as explained in the text.

phase, $E_S = (26 \pm 8)$ kJ mol^{-1} K^{-1}, $E_L = (11 \pm 4)$ kJ mol^{-1} K^{-1} in the chiral nematic phase, and $E_S = (30 \pm 8)$ kJ mol^{-1} K^{-1}, $E_L = (2 \pm 3)$ kJ mol^{-1} K^{-1} in the smectic A phase. As it can be noticed, E_L in the SmA phase was estimated with a large uncertainty due to the lack of T_1^{-1} experimental results at Larmor frequencies larger that 100 MHz.

The model fit in the isotropic phase shows that the OF contribution observed 5 K above the T_{IN^*} is much larger than the one observed for 5CB for the same $\Delta T = T - T_{IN}$ (see Figure 9a). Since $A_{OF} \sim T\eta_{iso}^{1/2}/K_{iso}^{3/2}$, this might correspond to a significant difference in the viscoelastic properties of 5CB* with respect to 5CB, in view of very different temperatures. The considerably smaller ω_0 obtained for 5CB* at $T - T_{IN} \sim 5$ K when compared with the value obtained for 5CB for the same ΔT (see Table 1 and Table 2) can be, therefore, associated with the different values of the viscoelastic parameters between the two LC systems and is not related with major differences in coherence length ξ values associated with the size of the clusters.

Due to the chiral nematic structure, the model fitted to the T_1^{-1} experimental results considers the RMTD contribution in addition to the SD, R, and ODF. However, it is clear that in view of the reported pitch value[9] and for reasonable values of the interproton distances this contribution is not important for the T_1^{-1} dispersion in the frequency range considered in this work, as observed in Figure 9b.

Table 2. Model Parameters Obtained from the Best Fits of Equation 7 to the Experimental T_1^{-1} Results in the Isotropic, Chiral Nematic, and SmA Phases of 5CB*[a]

phase	I	I	N*	SmA
T (K)	307	265	254	245
τ_S (10^{-09} s)	1.82 ± 0.07	~2.14	4.1 ± 0.6	3.2 ± 0.02
τ_L (10^{-10} s)	5.10 ± 0.01	~93	64 ± 9	67 ± 13
A_R (10^{-49} m^6 s^{-2})	~3.5	~3.5	~3.06	~3.0
D (10^{-12} m^2 s^{-1})	28	1.6	0.6 ± 1	0.10 ± 0.05
$\langle r^2 \rangle$ (10^{-20} m^2)	20 ± 5	20 ± 5	-	-
A_c (10^3 s$^{-3/2}$)	2.5 ± 0.5	181 ± 3	205 ± 6	-
A_{LU} (10^8 s^{-2})	-	-	-	2.84 ± 0.07
$\omega_0/2\pi$ (10^3 Hz)	806 ± 200	15 ± 1	-	-
$\omega_{cmin}/2\pi$ (10^4 Hz)	0	0	3.8 ± 0.3	20 ± 1
$\omega_{cmax}/2\pi$ (10^6 Hz)	7 ± 1	9 ± 1	11 ± 1	~20
p (10^{-6} m)	-	-	~0.3	-
r_{eff} (10^{-10} m)	-	-	~3.5	-

[a] Index c refers to the type of collective motions observed in each phase: local order fluctuations, OF, and order director fluctuations, ODF, in the chiral nematic phase. The value of the pitch p was obtained from ref 9.

It should be mentioned that the proton T_1^{-1} dispersion is strongly dominated by the ODF relaxation mechanism from low frequencies up to the megahertz range. This result is in agreement with the results found for the HZL 7/* compound[3] but in contrast with the published work on the BET cholesteric liquid crystal.[7] In the case of the BET N* phase, the T_1^{-1} dispersion in the whole frequency range was explained by a sum of SD, R, RMTD, and LU relaxation mechanisms. The inclusion of the LU contribution instead of the ODF was required since the authors did not include a finite value for the high cutoff frequency in their ODF model. This was equivalent to assume that $\omega_{ODFmax} \rightarrow \infty$ in eq 1. As we mentioned previously, ω_{ODFmax} can not be arbitrarily large. The value of $\omega_{ODFmax}/2\pi$ in the expected range of about 10 MHz would have made it possible to explain the experimental results within the scope of the ODF relaxation model.

The model fit for the SmA phase presented in Figure 10 was obtained considering the translation diffusion coefficient as a free fitting model parameter. The value obtained is smaller, by a factor of 2, than the value that we might estimate from the experimental self-diffusion results in the isotropic phase (see Figure 6). A slightly worse fit is obtained if the estimated value $D_\perp \sim 1.8 \times 10^{-13}$ m^2 s^{-1} is used instead. The main consequence is the small decrease of the low cutoff frequency value. The remaining model parameters are not significantly affected.

The factor of 2 found between the value of $D_\perp$ obtained from the model fit (see Table 2) and the value estimated from the diffusion measurements (see Figure 6) shows that in the low frequency range of the T_1^{-1} dispersion the SD relaxation contribution might be overestimated. In the N* phase this is not the case since the estimated value for $D_\perp$ in this mesophase (see Figure 6) is very close to the value obtained from the model fit that considers $D_\perp$ as a free model parameter in the fit.

It is worthwhile to mention the important contribution of layer undulations to the T_1^{-1} dispersion over a broad frequency range

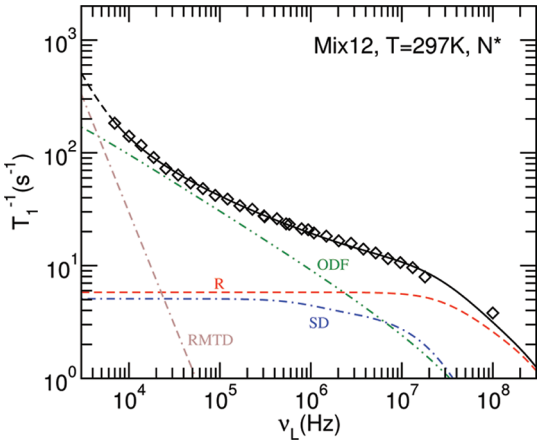

Figure 12. Experimental T_1^{-1} dispersion results in the nematic phase of the Mix12 LC system and the best model fit curves obtained with the relaxation model given by eq 7 as explained in the text.

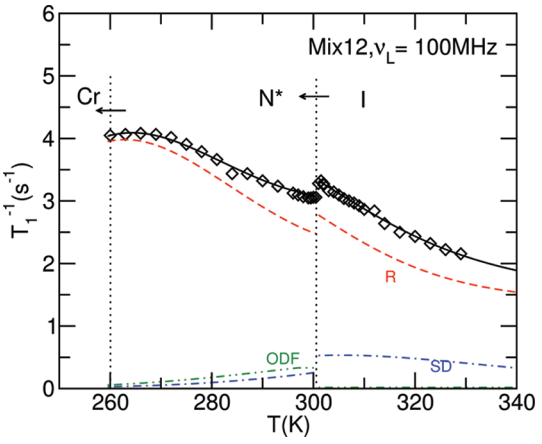

Figure 13. Experimental results of T_1^{-1} as function of the temperature for the Mix12 LC system and the best model fit curves obtained with the relaxation model given by eq 7 as explained in the text.

that extends from low frequencies up to 10 MHz. To the authors knowledge, this is the first observation of such a T_1^{-1} dispersion behavior in the SmA phase for a low molecular weight liquid crystal. Previous observations of layer undulations as the main relaxation mechanism over a broad frequency range were reported for the SmA and SmC phases of liquid crystals of tetrapode molecules (low generation dendrimers)[37] and, more recently, for a TGBC-like phase of a chiral liquid crystal with a different molecular core and longer chains.[3] The A_{LU} value obtained for the 5CB* SmA phase is one order of magnitude larger than the value obtained in the SmA phase of the tetrapode LC[37] and much larger than the values found for SmA phases of other low molar mass LCs.[14,15] The large A_{LU} value obtained seems to point to a smaller coherence length ξ_z, associated with the number of layers involved in the collective fluctuations, in comparison with the values found for other LC systems, considering identical values for the viscoelastic parameters.

The T_1^{-1} temperature dependence is very well explained by the relaxation model, as can be observed in Figure 11. At 100 MHz, the longitudinal relaxation rate is dominated by the rotations/reorientations relaxation contribution with some minor contributions from the other relaxation mechanisms. One consequence of this is the large uncertainty associated with temperature dependence of the fitting parameters A_c and ω_{cmin} (or ω_0). In fact, these parameters were considered fixed in the temperature dependence fits of the T_1^{-1} results in the 5CB* mesophases. In the isotropic phase, the values of A_c and ω_0 could only be obtained for the temperatures 307 and 265 K (see Table 2).

It is interesting to observe that the values of the activation energies obtained from the model fits are not the same in all 5CB* mesophases. In particular, E_S seems to increase with the increasing order of the phase. E_L presents the opposite behavior, and its value is larger in the isotropic phase than in the SmA phase, meaning that molecular rotations along the long molecular axis are more hindered in the isotropic phase. Molecular reorientations around the short molecular axis are more hindered in the SmA phase than in the isotropic phase.

Mix12 LC System Data Analysis. The T_1^{-1} frequency and temperature dependencies in all phases of the Mix12 mixture were analyzed taking into account the model given by eq 7 with the following fitting parameters: A_R, τ_S, E_S, τ_L, E_L, $\langle r^2\rangle_{iso}$, A_c, ω_{cmax}, ω_{cmin}, A_{RMTD}. The value of the pitch was estimated from the POM optical textures (see Figure 2), $p \sim 3.1 \times 10^{-6}$ m. Index c stands for OF or ODF, according to the type of collective motions observed in each phase. In view of the small percentage of 5CB* in 5CB, it is assumed that the order parameter S has the same temperature dependence as for 5CB. In addition, the translational self-diffusion coefficients in the N* phase were estimated from the values measured in the isotropic phase of the mixture. The temperature dependence of the fitting parameters of the OF or ODF relaxation mechanisms could not be obtained since the $T_1^{-1}(T)$ was measured at 100 MHz, and as seen before for the 5CB and 5CB* systems, these contributions are very small at high frequencies.

Table 3. Model Parameters Obtained from the Best Fits of Equation 7 to the Experimental T_1^{-1} Results in the Isotropic and Chiral Nematic Phases of the Mix 12 LC System[a]

phase	I	N*
T (K)	307	297
τ_S (10^{-09} s)	2.1 ± 0.2	2.4 ± 0.2
τ_L (10^{-10} s)	8.4 ± 0.5	9.8 ± 0.02
A_R (10^{-49} m^6 s^{-2})	3.6	3.6
$\langle r^2\rangle$ (10^{-20} m^2)	~25	-
A_c (10^3 s$^{-3/2}$)	25 ± 2	9.8 ± 0.3
$\omega_0/2\pi$ (10^3 Hz)	580 ± 8	-
$\omega_{cmin}/2\pi$ (10^3 Hz)	0	<1
$\omega_{cmax}/2\pi$ (10^8 Hz)	~0.1	~1.6

[a] Index c refers to the type of collective motions observed in each phase: local order fluctuations, OF, in the isotropic phase and order director fluctuations, ODF, in the nematic phase.

The best fit obtained in the N* phase, 5 K below the T_{IN} phase transition, is presented in Figure 12. The temperature dependence fits in the isotropic and nematic phases are presented in Figure 13. The model fit of the T_1^{-1} dispersion in the isotropic phase is almost identical to the one obtained in the isotropic phase of 5CB and is not presented here (see the Supporting Information). The fitting parameters are presented in Table 3. The activation energies estimated from the temperature dependence fits were: $E_S = (10 \pm 22)$ kJ mol^{-1} K^{-1}, $E_L = (51 \pm 44)$ kJ mol^{-1} K^{-1} in the isotropic phase, $E_S = (8.7 \pm 7)$ kJ mol^{-1} K^{-1}, $E_L = (27 \pm 3)$ kJ mol^{-1} K^{-1} in the nematic phase. The estimated

fitting errors for the activation energies are considerably larger and reflect not only the interdependence of extracted fitting parameter values but also the fact that the temperature range was not large enough to independently estimate E_S and E_L. The activation energy considered for the translational self-diffusion was obtained from the Arrhenius curve fit to the experimental results obtained for the self-diffusion constant in the isotropic phase (see Figure 6).

Contrary to 5CB*, the T_1^{-1} dispersion observed in Figure 12 clearly requires the contribution of the RMTD relaxation mechanism at low frequencies. Assuming the value of the pitch obtained from the analysis of the POM textures, the value of the effective interproton distance estimated from the RMTD model is slightly smaller than the value considered in the N* phase of the pure 5CB* compound. These differences might be related to the slightly different molecular structures of 5CB and 5CB* molecules due to the presence of the methyl group in the 5CB* aliphatic chain and the fact that the 5CB* concentration in the mixture is relatively small.

The temperature dependence is well explained by the T_1^{-1} model. The temperature dependence at 100 MHz is clearly dominated by the rotations/reorientations contribution in both the isotropic and chiral nematic phases.

The ODF contribution to the T_1^{-1} temperature dependence in the N* phase, at 100 MHz, decreases with decreasing temperature as observed also in the N phase of the pure 5CB. This does not correspond to a decrease of the ODF prefactor but to the expected decrease of the high cutoff frequency value with decreasing temperature, as explained previously.

The activation energies for the rotations/reorientations obtained from the T_1^{-1} temperature dependence fits are close to the ones obtained for the pure 5CB system. As for that system, the E_S and E_L values obtained in the isotropic phase of the mixture are larger than the ones obtained for the N* phase. The values of E_L are larger than the values of E_S in both phases, as well. Nevertheless, it is interesting to observe that in the isotropic phase of the mixture the value of E_L is larger than the one found for 5CB in the same phase. On the contrary, in the nematic phase, the value of E_L is smaller than the one obtained for 5CB. This follows closely the E_L differences detected between 5CB and 5CB* since $E_L^{5CB*} > E_L^{5CB}$ in the isotropic phase and $E_L^{5CB*} < E_L^{5CB}$ in the nematic phase.

CONCLUSIONS

In this work, we present a comprehensive study of the molecular dynamics in three liquid crystalline systems: 5CB, 5CB*, a chiral compound with a molecular structure very similar to the one of 5CB, and a mixture of 12% (w/w) of 5CB* in 5CB. The spin−lattice relaxation time was measured over a broad frequency range from 100 MHz down to 5 kHz. In addition, the T_1 temperature dependence was also obtained in the isotropic and in all mesophases of the studied systems.

The experimental results were analyzed using a model that takes into account the relevant relaxation mechanisms considering the structural aspects of each phase and the temperature and frequency ranges covered. In the isotropic phase of the three systems, these relaxation mechanisms correspond to local molecular rotations/reorientations, translational self-diffusion, and, close to T_{I-N}, order fluctuations. In the nematic and smectic A phases the nature of the collective motions is different than those observed in the isotropic phase and presents clearly different T_1^{-1} dispersion signatures. Order director fluctuations and layer undulations were detected in nematic (and also chiral nematic) and smectic A phases, respectively.

In the chiral nematic phase, an additional relaxation mechanism was included to account for the particular diffusion and rotation of the molecules observed in the direction parallel to the helical axis.

The relaxation model was fitted to the experimental results of 5CB, and the values of the fitting parameters were analyzed in agreement with the 5CB physical constants found in the literature. The values obtained for the rotations/reorientations correlation times are compatible with others found in the literature for this compound.

The analysis of the 5CB* experimental results was analyzed considering that in the chiral nematic phase the rotations induced by translational displacements can contribute to the relaxation with a correlation time distinct from the one associated with the translational self-diffusion process found in the nematic phases. However, in view of a very small pitch this relaxation mechanism is not relevant for the spin−lattice relaxation in the whole frequency range considered in this study. In the case of the smectic phase, the collective motion contributions are clearly associated with layer undulations with the characteristic $T_1^{-1} \sim \nu_L^{-1}$ frequency dependence, as found for all smectic A phase T_1^{-1} dispersion profiles. It is important to stress that in the case of 5CB* the frequency region where this contribution is the most relevant for the relaxation is not restricted only to frequencies below the tens of kilohertz, as it is more commonly observed, but it extends to frequencies up to 10 MHz. This is the first time such behavior is observed on a low molecular weight calamitic liquid crystal.

The spin−lattice relaxation measured for the 5CB*/5CB mixture as a function of the Larmor frequency and temperature was analyzed in terms of the relaxation mechanisms also used to interpret the results obtained for the pure 5CB* liquid crystalline system. As expected, the 12% (w/w) 5CB* in the 5CB liquid crystalline mixture presents a chiral nematic phase with a helical pitch much larger that the one found in the N* phase of pure 5CB*. The T_1^{-1} dispersion results obtained for this mixture clearly show that at low frequencies the frequency dependence follows a power law which is not observed in the nematic phase of pure 5CB nor in the N* phase of the pure 5CB* for the same temperature difference with respect to T_{I-N}. The T_1^{-1} relaxation dispersion is clearly compatible with the inclusion of the RMTD relaxation mechanism contribution in the relaxation model considering the value of the pitch estimated by POM.

ASSOCIATED CONTENT

Supporting Information. Relaxation models, analysis of 5CB T_1^{-1} experimental results, analysis of 5CB* T_1^{-1} experimental results, and synthesis of 5CB*. This material is available free of charge via the Internet at http://pubs.acs.org.

AUTHOR INFORMATION

Corresponding Author

*E-mail: pedro.jose.sebastiao@ist.utl.pt; tomaz.apih@ijs.si; mhg@fct.unl.pt.

ACKNOWLEDGMENT

The authors wish to thank the Portuguese Fundação para a Ciência e a Tecnologia (FCT) for the financial support

through Portuguese−Slovenian bilateral project and through FCT contract PTDC/CTM/099595/2008. Luís Pinto acknowledges FCT grant SFRH/BDP/65133/2009.

REFERENCES

(1) Dong, R. *Nuclear magnetic resonance of liquid crystals*; Springer: New York, 1997.
(2) Sebastião, P.; Cruz, C.; Ribeiro, A. Advances in Proton NMR Relaxometry in Thermotropic Liquid Crystals. In *Nuclear magnetic resonance spectroscopy of liquid crystals*; Dong, R. Y., Ed.; World Scientific Co.: River Edge, NJ, 2009; Chapter 5, pp 129−167.
(3) Apih, T.; Domenici, V.; Gradišek, A.; Hamplova, V.; Kaspar, M.; Sebastião, P. J.; Vilfan, M. *J. Phys. Chem. B* **2010**, *114*, 11993–12001.
(4) Dong, R. Y.; Pintar, M. M.; Forbes, W. F. *J. Chem. Phys.* **1971**, *55*, 2449.
(5) Tarr, C. E.; Field, M. E. *Mol. Cryst. Liq. Cryst.* **1975**, *30*, 143–148.
(6) Vilfan, M.; Blinc, R.; Dolin.ek, J.; Ipavec, M.; Lahajnar, G.; Žumer, S. *J. Phys. (Paris)* **1983**, *44*, 1179–1184.
(7) Pusiol, D.; Noack, F.; Aguilera, C. *Z. Naturforsch., A* **1990**, *45*, 1077–1084.
(8) Humar, M.; Musevic, I. *Opt. Express* **2010**, *18*, 26995–27003.
(9) W., G. G.; McDonnell, D. G. *Mol. Cryst. Liq. Cryst.* **1976**, *37*, 189–211.
(10) Nakamura, Y.; Mori, K. *Eur. J. Org. Chem.* **1999**, *9*, 2175–2182.
(11) Noack, F. *Prog. Nucl. Magn. Reson. Spectrosc.* **1986**, *18*, 171–276.
(12) Kimmich, R.; Anoardo, E. *Prog. Nucl. Magn. Reson. Spectrosc.* **2004**, *44*, 257–320.
(13) Pusiol, D.; Noack, F. *Liq. Cryst.* **1989**, *5*, 377–387.
(14) Sebastião, P. J.; Ribeiro, A. A. C.; Nguyen, H. T.; Noack, F. *J. Phys. II* **1995**, *5*, 1707–1724.
(15) Carvalho, A.; Sebastião, P. J.; Ribeiro, A. C.; Nguyen, H. T.; Vilfan, M. *J. Chem. Phys.* **2001**, *115*, 10484–10492.
(16) Filip, D.; Cruz, C.; Sebastião, P. J.; Cardoso, M.; Ribeiro, A. C.; Vilfan, M.; Meyer, T.; Kouwer, P. H. J.; Mehl, G. H. *Phys. Rev. E* **2010**, *81*, 011702.
(17) Kimmich, R.; Unrath, W.; Schnur, G.; Rommel, E. *J. Magn. Reson.* **1991**, *91*, 136–140.
(18) Apih, T.; Khare, V.; Klanjšek, M.; Jeglič, P.; Dolinšek, J. *Phys. Rev. B* **2003**, *68*, 212202.
(19) Torrey, H. C. *Phys. Rev.* **1953**, *92*, 962.
(20) Žumer, S.; Vilfan, M. *Phys. Rev. A* **1978**, *17*, 424–433.
(21) Vilfan, M.; Žumer, S. *Phys. Rev. A* **1980**, *21*, 672–680.
(22) Woessner, D. E. *J. Chem. Phys.* **1962**, *36*, 1.
(23) Sebastião, P. J.; Godinho, M. H.; Ribeiro, A. C.; Guillon, D.; Vilfan, M. *Liq. Cryst.* **1992**, *11*, 621–635.
(24) Vilfan, M.; Apih, T.; Sebastião, P. J.; Lahajnar, G.; Žumer, S. *Phys. Rev. E* **2007**, *76*, 051708.
(25) Sebastião, P. J.; Sousa, D.; Ribeiro, A. C.; Vilfan, M.; Lahajnar, G.; Seliger, J.; Žumer, S. *Phys. Rev. E* **2005**, *72*, 061702.
(26) de Gennes, P. G. *The Physics of Liquid Crystals*; Clarendon Press: Oxford, 1974.
(27) Pincus, P. *Solid State Commun.* **1969**, *7*, 415.
(28) Wölfel, W.; Noack, F.; Stohrer, M. Z. *Naturforsch. A* **1975**, *30*, 437.
(29) Dvinskikh, S. V.; Furo, I.; Zimmermann, H.; Maliniak, A. *Phys. Rev. E* **2002**, *65*, 061701.
(30) Haller, I. *Prog. Solid State Chem.* **1975**, *10*, 103–118.
(31) Sebastião, P. J. http://fitter.ist.utl.pt, 2009.
(32) Chmielewski, A. G.; Lepakiewicz, E. *Rheol. Acta* **1984**, *23*, 207–210.
(33) Bunning, J. D.; Faber, T. E.; Sherrell, P. L. *J. Phys.* **1981**, *42*, 1175–1182.
(34) Beckmann, P. A.; Emsley, J. W.; Luckhurst, G. R.; Turner, D. L. *Mol. Phys.* **1986**, *59*, 97.
(35) Dong, R. Y. *Phys. Rev. E* **1998**, *57*, 4316–4322.
(36) Struppe, J.; Noack, F. *Liq. Cryst.* **1996**, *20*, 595–606.
(37) Filip, D.; Cruz, C.; Sebastião, P. J.; Ribeiro, A. C.; Vilfan, M.; Meyer, T.; Kouwer, P. H. J.; Mehl, G. H. *Phys. Rev. E* **2007**, *75*, 11704.